Nanoscale

Accepted Manuscript

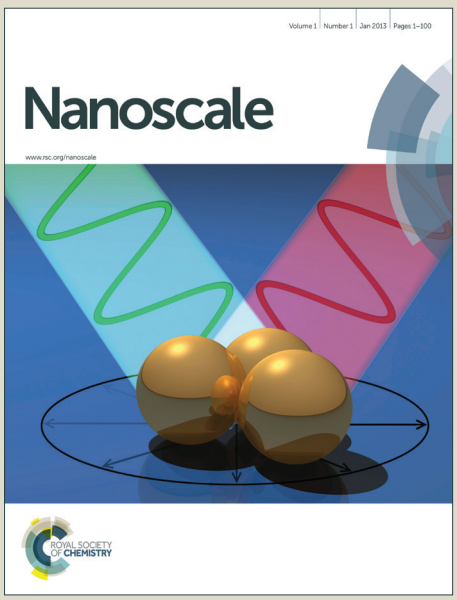

ROYAL SOCIETY OF CHEMISTRY

www.rsc.org/nanoscale

Journal Name

COMMUNICATION

Universal chitosan-assisted synthesis of Ag-included heterostructured nanocrystals for label-free in situ SERS monitoring

Received 00th January 20xx,
Accepted 00th January 20xx

DOI: 10.1039/x0xx00000x

www.rsc.org/

Kai Cai,‡ Xiaoyan Xiao,‡ Huan Zhang, Zhicheng Lu, Jiawei Liu, Qin Li, Chen Liu, Mohamed F. Foda and Heyou Han*

A universal chitosan-assisted method was developed to synthesize various Ag-included heterostructured nanocrystals, in which chelation probably plays a vital role. The as-prepared Ag/Pd heterostructured nanocrystals show outstanding properties when being used as bifunctional nanocomposites in label-free in situ SERS monitoring of Pd-catalytic reaction.

Surface-enhanced Raman scattering (SERS) possesses inherent advantages in label-free in situ monitoring the catalytic reaction process, which can help to understand the reaction mechanism and optimize the catalyst formula.[1-5] It is well known that some noble metal structures, such as Ag and Au nanocrystals, are required for magnifying the molecule information in the SERS process.[5-9] Moreover, SERS is a short-range effect, and the catalytic reaction is a process taking place at the surface of the catalyst. Hence, assembling nanocrystals with SERS activity and catalyst together is significant for realizing an accurate and highly effective monitoring.

Recently, various protocols in fabricating the bifunctional units, which combine both catalytic and SERS activity, have been developed for label-free in situ monitoring.[3,5,7,8,10-16] A general strategy to fabricate the units is to coat a SERS-active core with a catalytically active surface, including assembling small Au nanoparticles (NPs) on the core or coating the core with a shell of Pt or Pd.[4,5,10,11,17] However, it is difficult to achieve a balance between high catalytic efficiency and SERS enhancement in this method, as the plasmon of the core will be significantly decreased with the increase of shell thickness.[4,12,17]

In addition, other methods, such as depositing isolated Au NPs and Pt NPs simultaneously onto the glass substrate to study Pt-catalyzed reaction, provide a different route.[1] But the non-chemically bound metal nanoparticles are unpractical as a system under real catalytic conditions.[3] It is known that Au core is the most employed materials in the fabrication of bifunctional units, including Au nanorods and nanowires.[3-8,10,11,18-20] In fact, Ag has a stronger localized surface plasmon resonance (LSPR) and can provide a higher enhancement factor than Au even though the latter is more chemically inert, which is an advantage in assembling bifunctional structures.[17,21-23]

Heterogeneous metal nanocrystals (HMNCs) are a common entity formed by integrating some metal nanocrystals of different compositions, which are jointed through permanent bonding interfaces.[24-29] Particularly, the oligomer-type HMNCs, which are different from the core-shell type ones, expose multiple material surfaces, which can avoid the dilemma in keeping the balance between catalytic and SERS activity.

Pd and Pt are the most important catalysts in many applications, including the conversion of chemical to electrical energy and a series of vital organic chemical reactions.[30-31] Therefore, it is highly desirable to synthesize oligomer-type HMNCs containing Ag and Pd (Pt) and use them as the substrate for the lable-free in situ SERS monitoring.

Herein, we demonstrate a facile synthesis of Ag/Pd oligomer-type heterostructured nanotubes (OHNTs), in which some Ag NPs are jointed to a one-dimensional (1D) Pd nanotubes (NTs) through permanent bonding interfaces. Chitosan plays a vital role in the successful preparation of Ag/Pd OHNTs; Without chitosan, Ag could not heterogeneously nucleate and grow on the NTs uniformly. The method was then successfully used to grow Ag NPs on bimetallic NTs, such as PdPt alloy NTs or quasi-1D Au/PtAu heterojunction NTs. Finally, Ag/Pd OHNTs were used to monitor the reaction process of p-nitrothiophenol (p-NTP) to p-aminothiophenol (p-ATP) in label-free in situ by SERS in aqueous solution.

The Te nanowires (NWs) were synthesized at first. Then the Pd NTs were synthesized by using Te NWs as the template and chitosan as the stabilizing agent in aqueous solution at room temperature. The TEM images of the as-prepared Te NWs and Pd NTs are shown in Fig. S1 and 1A, respectively. It is shown that Pd NTs have the same size with Te NWs template (about 30 nm in diameter and 420 nm in length), and it can be observed that the centers of the 1D Pd nanostructures are obviously brighter than the edges, suggesting that they are hollow nanotubes. The XRD pattern of the Pd NTs (Fig. S2) shows a characteristic diffraction peak which can be assigned to

State Key Laboratory of Agriculture Microbiology, College of Food Science and Technology, College of Science, Huazhong Agricultural University, Wuhan 430070, China. E-mail: hyhan@hzau.edu.cn

‡ Equal contribution.

Electronic Supplementary Information (ESI) available: [details of any supplementary information available should be included here]. See DOI: 10.1039/x0xx00000x

the (111) lattice plane of face-centered-cubic (fcc) Pd structures. The other peaks of fcc Pd were not obviously observed, which might

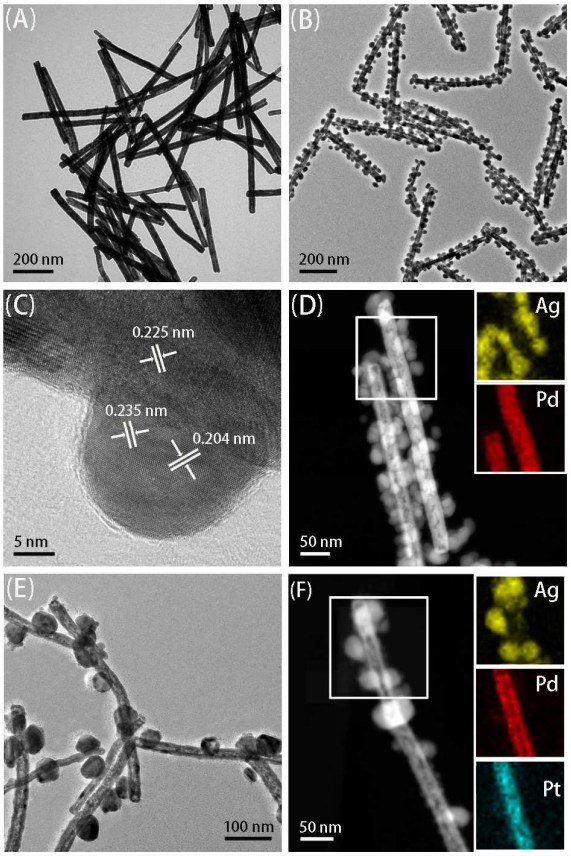

Fig. 1 TEM images of Pd NTs (A), Ag/Pd OHNTs (B), Ag/PdPt OHNTs (E). HRTEM images of Ag/Pd OHNTs (C). HAADF-STEM images of Ag/Pd OHNTs (D), Ag/PdPt OHNTs (F).

be caused by a lack of other planes with appropriate area.

Ag NPs grow on the Pd NTs by reducing silver nitrate with ascorbic acid in the chitosan and PVP solution. The typical TEM image of Ag/Pd OHNTs is shown in Fig. 1B. Some 0-dimensional (0D) nanocrystals with a diameter of 30 nm grow up on the surface of a 1D Pd NTs. The HRTEM image of Ag/Pd OHNTs (Fig. 1C) shows that the attached NPs are jointed to the Pd NTs through permanent bonding interfaces and a crystal boundary can be clearly observed. One of the interplanar spacings of the nanotube is about 0.225 nm, which is consistent with the (111) lattice plane of fcc Pd, and 0.235 and 0.204 nm in the particles are corresponding to the (111) and (200) lattice planes of fcc Ag, respectively. In addition, the high-angle annular dark-field scanning TEM-energy-dispersive X-ray spectroscopy (HAADF-STEM-EDS) elemental mapping image of the Ag/Pd OHNTs shows the distinct compositional distribution of each constituent metal element (Fig. 1D). It unambiguously reveals that Ag NPs are linked onto the 1D Pd NTs skeleton. The energy-dispersive X-ray spectroscopy (EDS) performed on Pd NTs (Fig. S3) shows that they are mainly composed of Pd and Ag elements. The presence of a few Te elements indicates that the used templates are Te NWs. When the amount of Pd precursor used in the synthesis of Pd NTs was adjusted, the Te elements might be completely absent. The XRD pattern of the Ag/Pd OHNTs (Fig. S2) shows more characteristic diffraction peaks than the last one, which can be suitably assigned to the reflections from the fcc structure of Ag. When Pd and Pt precursors were added simultaneously instead of single Pd precursor using the same method, PdPt bimetallic NTs were obtained (Fig. S4). According to inductively coupled plasma atomic emission spectrometer (ICP-AES) analysis, the molar ratio of Pd : Pt is about 7 : 1. The TEM images of the as-prepared Ag/PdPt OHNTs show that they have the same morphology with Ag/Pd OHNTs (Fig. 1E). Moreover, HAADF-STEM-EDS was used to further characterize the structure. As shown in Fig. 1F, Ag elements are distributed on NPs while both of Pd and Pt elements are distributed on NTs, revealing that Ag NPs are linked onto the 1D PdPt bimetallic NTs skeleton. The EDS performed on Ag/PdPt OHNTs (Fig. S5) shows that they are composed of Pd, Pt and Ag elements, but no Te element was observed.

In order to investigate the role of chitosan in the synthesis of heterostructured nanocrystals, a contrast test was performed. Porous PdPt NTs were synthesized using Te NWs as templates in the hexadecyltrimethylammonium bromide (CTAB) solution, and were then used as the intermediate for the following synthesis (Fig. S6). ICP-AES analysis shows that the molar ratio of Pd : Pt in the NTs is about 11 : 9. When chitosan was used as surfactant, as shown in Fig. 2A, all of the Ag NPs are jointed on the porous PdPt NTs. In Fig. 2B, HAADF-STEM-EDS further demonstrates that the Ag NPs are jointed on the PdPt NTs, and the EDS analysis (Fig. S7) shows that they are composed of Pd, Pt and Ag elements. However, when using polyvinyl pyrrolidone (PVP) as surfactant instead of using chitosan, Ag NPs can not grow uniformly on the surface of the porous PdPt NTs. A typical result is shown in Fig. 2C: Ag NPs tend to aggregate and are not well-distributed. To further understand the effect, we tested other surfactants in the synthesis instead of chitosan, such as

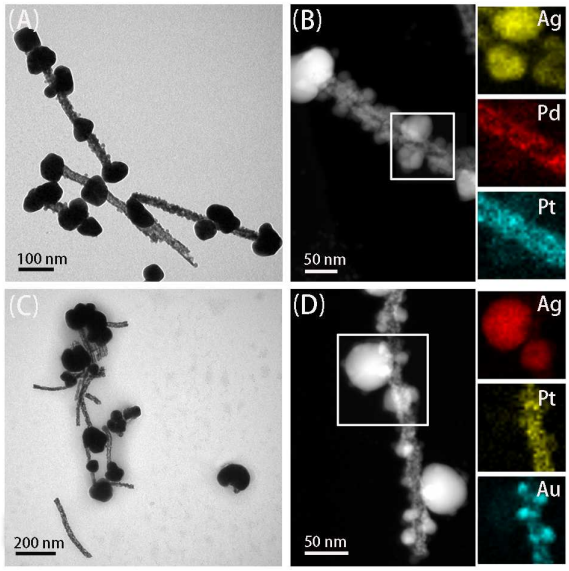

Fig. 2 TEM images of Ag/PdPt OHNTs using chitosan (A) and PVP (C) as surfactants in the synthesis. HAADF-STEM images of

Ag/PdPt OHNTs (B) and Ag/Au/PtAu heterostructured nanotubes (D).

CTAB, sodium dodecyl sulfate (SDS) and acrylic acid polymers (PAA) (Fig. S8). Probably because of the electrostatic repulsion of CTAB and Ag ion or the termination of growth of little Ag NPs by CTAB, no Ag NPs appear clearly on nanotubes. Even though SDS exhibit negative charge and Ag ions can absorb on the nanotubes, not all Ag NPs are grown on the nanotubes. Moreover, PAA has a same performance with SDS because it is also of negative electricity. Chitosan is a polysaccharide biopolymer formed by the deacetylation of naturally occurring chitin with a large number of functional groups. Although it is of positive charge as CTAB, it possesses unique polycationic and chelating properties.[32-33] In this research, chelation induced the even dispersion of Ag ions on the surface of the metal NPs, which probably provides the essential conditions for the heterogeneous nucleation and growth of Ag on the NPs. In addition, adhesion may have certain effect on the process. Therefore, we can conclude that chitosan plays a vital role in the preparation of Ag-included heterostructured nanocrystals.

In addition, to further confirm the method, a more complicated heterostructure, Au/PtAu heterostructured NTs, was used as the intermediate to fabricate Ag-included heteronanostructures. The Au/PtAu heterostructured NTs were prepared firstly (Fig. S9), and were then used in the next process. The TEM image demonstrates that Ag-included heterostructures were obtained (Fig. S10). HAADF-STEM-EDS was also used to test the result. As shown in Fig. 2D, Ag NPs are obviously linked on the surface of the PtAu NTs. The EDS performed on the structures shows that they are composed of Au, Pt and Ag elements (Fig. S11). Even though Ag and Au crystals have a higher match than Ag and Pt crystal, at the presence of chitosan, it was not observed that more Ag NPs were linked to Au NPs than to PtAu NTs framework as expected. When using PVP instead of chitosan in the synthesis, we found that Ag NPs apparently were not well-distributed on the surface of Au/PtAu heterostructured NTs (Fig. S12). All these results demonstrate that chitosan is vital in the heterostructured growth of Ag NPs on other materials and the chitosan-assisted method is a universal strategy to obtain Ag-included heterostructures.

It is well known that many noble metal NPs can catalyze the reaction of p-NTP to p-ATP. Herein, UV-vis absorption spectra were used to testify the catalytic properties of the Ag/Pd heterostructured nanocrystals. As shown in Fig. 3, the absorption intensity of p-NTP at wavelength 410 nm decreases over time in the presence of the Ag/Pd heterostructured nanocrystals, while the contrast experiment shows no change (Fig. S13). Obviously, the as-prepared Ag/Pd heterostructured nanocrystals have catalytic activity towards the reaction of p-NTP to p-ATP. This result is in conformity with the anticipation, as only part of the surface of the Pd NTs is covered by Ag NPs and considerable Pd atoms are exposed to the solution. When the borohydride ions reacted with Pd, the electrons from the donor were relayed to the acceptor p-NTP right after both of them were absorbed onto the particle surfaces.

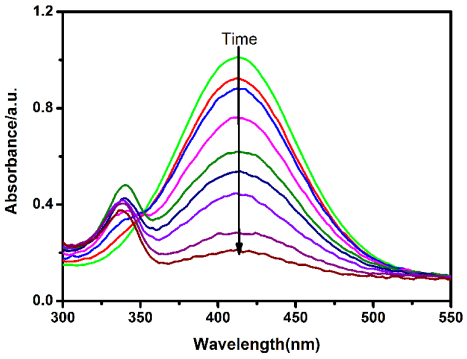

Fig. 3 Time dependent UV-vis absorption spectra for the reduction of p-NTP by $NaBH_4$ in the presence of Ag/Pd OHNTs. The absorption spectra were recorded every 3-4 min.

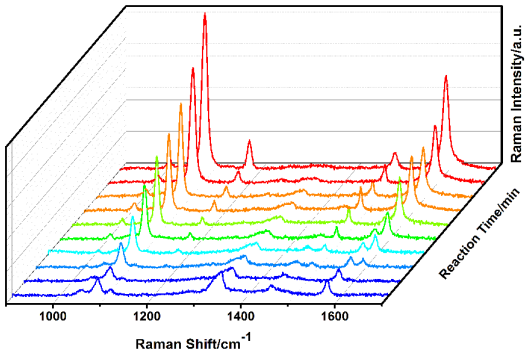

Fig. 4 SERS spectra recorded from the reaction suspension collected at different reaction times. From bottom to top: SERS spectra recorded at 0, 1, 2, 3, 4, 5, 6, 7, 8 and 12 min after addition of $NaBH_4$ solution.

After the catalytic activity was determined, the SERS sensitivity was assessed. A series of Raman spectra were collected from the reaction system in sequence after the addition of $NaBH_4$. It is noteworthy that all samples were measured in aqueous solution without special mixture process in our study, both of which are significant for a label-free in situ monitoring of the metal-catalytic reaction process by recording the SERS response in real time. As shown in Fig. 4, four characteristic peaks at 1082, 1113, 1345 and 1572 cm^{-1} of the bottom spectra are clearly observed, which are in accordance with those of pure p-NTP. As time went on, the characteristic peaks at 1345 and 1572 cm^{-1}, which correspond to R-NO_2 of p-NTP, gradually deceases and vanishes at last, while two new peaks at 1007 and 1590 cm^{-1}, which correspond to phenyl ring modes of p-ATP, were clearly observed. Generally, the intensity ratios of the peaks at 1572 and 1590 cm^{-1} were used to monitor the catalytic reaction. From the inexistence of the peak at 1590 at the beginning to the vanishing of the peak at 1572 at last, the essential reaction process was recorded by SERS in the experiment (Fig. S14). Because both the catalytic reaction and SERS took place at the surface of nanocrystals, we directly measured the samples in

aqueous solution without washing the p-NTP after a mixture process.

It is worth to point out that no peaks of p,p'-dimercapto-azobenzene (DMAB), which usually emerge in the reaction by various catalysts, were observed in the process. Moreover, PdAg bimetallic nanofibers were used as catalyst in the same reaction and intermediate product was observed in the process.[17] However, the PdAg heterostructures produced a different result in this work, even though a high laser power was used, which usually assists the production of the photo-chemical product.[5,34] Xie *et al.* reported that the production of intermediate product can be avoided by using a thin layer silica shell to isolate the inert Au core from the actual catalytic Au satellites.[7] Herein, we consider that the structural features of the catalyst are probably an important reason for the non-appearance of the reaction intermediate.

In conclusion, we demonstrate a universal chitosan-assisted method for the facile synthesis of Ag-included heterostructured nanocrystals in aqueous solution at room temperature. Chitosan promotes the heterostructured nucleation and growth of Ag on other nanostructures in the synthesis. The as-prepared Ag/Pd heterostructured nanocrystals were used to monitor the reaction process of p-NTP to p-ATP by SERS in real time in aqueous solution successfully. The superior properties of the bifunctional nanocomposites exhibit great potentials in label-free in situ SERS monitoring of Pd-catalytic reaction. The design concept described here can also be extended to other bi- or tri-metallic NPs according to the actual requirement of the study on metal-catalytic reaction in situ by SERS.

The authors acknowledge financial support from the National Natural Science Foundation of China (21375043, 21175051) and the Doctor Innovation Project of Huazhong Agricultural University (0900205179).

Notes and references

1 V. Joseph, C. Engelbrekt, J. Zhang, U. Gernert, J. Ulstrup and J. Kneipp, *Angew. Chem., Int. Ed.*, 2012, **51**, 7592.
2 D. Wu, L. Zhao, X. Liu, R. Huang, Y. Huang, B. Ren and Z. Tian, *Chem. Commun.*, 2011, **47**, 2520.
3 Q. Cui, A. Yashchenok, L. Zhang, L. Li, A. Masic, G. Wienskol, H. Möhwald and M. Bargheer, *ACS Appl. Mater. Interfaces*, 2014, **6**, 1999.
4 R. Liu, J.-F. Liu, Z.-M. Zhang, L.-Q. Zhang, J.-F. Sun, M.-T. Sun and G.-B. Jiang, *J. Phys. Chem. Lett.*, 2014, **5**, 969.
5 J. Huang, Y. Zhu, M. Lin, Q. Wang, L. Zhao, Y. Yang, K. X. Yao and Y. Han, *J. Am. Chem. Soc.*, 2013, **135**, 8552.
6 Y.-C. Tsao, S. Rej, C.-Y. Chiu and M. H. Huang, *J. Am. Chem. Soc.*, 2014, **136**, 396.
7 W. Xie, B. Walkenfort and S. Schlücker, *J. Am. Chem. Soc.*, 2013, **135**, 1657.
8 W. Xie, C. Herrmann, K. Kömpe, M. Haase and S. Schlücker, *J. Am. Chem. Soc.*, 2011, **133**, 19302.
9 R. A. Álvarez-Puebla, R. Contreras-Cáceres, I. Pastoriza-Santos, J. Pérez-Juste and L. M. Liz-Marzán, *Angew. Chem., Int. Ed.*, 2009, **48**, 138.
10 Z. Y. Bao, D. Y. Lei, R. Jiang, X. Liu, J. Dai, J. Wang, H. L. W. Chan and Y. H. Tsang, *Nanoscale*, 2014, **6**, 9063.
11 Q. Cui, G. Shen, X. Yan, L. Li, H. Möhwald and M. Bargheer, *ACS Appl. Mater. Interfaces*, 2014, **6**, 17075.
12 W. Cai, X. Tang, B. Sun and L. Yang, *Nanoscale*, 2014, **6**, 7954.
13 X. Tang, W. Cai, L. Yang and J. Liu, *Nanoscale*, 2014, **6**, 8612.
14 X. Liang, T. You, D. Liu, X. Lang, E. Tan, J. Shi, P. Yin and L. Guo, *Phys. Chem. Chem. Phys.*, 2015, **17**, 10176.
15 G. Zheng, L. Polavarapu, L. M. Liz-Marzán, I. Pastoriza-Santos and J. Pérez-Juste, *Chem. Commun.*, 2015, **51**, 4572.
16 D. Qi, X. Yan, L. Wang and J. Zhang, *Chem. Commun.*, 2015, **51**, 8813.
17 M. Cao, L. Zhou, X. Xu, S. Cheng, J.-L. Yao and L.-J. Fan, *J. Mater. Chem. A*, 2013, **1**, 8942.
18 Y. Wang, Y.-Q. Wang, B. Yan and L.-X. Chen, *Chem. Rev.*, 2013, **113**, 1391.
19 J.-R. Li, G.-G. Zhang, L.-H. Wang, A.-G. Shen and J.-M. Hu, *Talanta*, 2015, **140**, 204.
20 M. Lin, Y.-Q. Wang, X.-Y. Sun, W.-H. Wang and L.-X. Chen, *ACS Appl. Mater. Interfaces.*, 2015, **7**, 7516.
21 T. Yang, H. Yang, S. J. Zhen and C. Z. Huang, *ACS Appl. Mater. Interfaces*, 2015, **7**, 1586.
22 M. Potara, A. Gabudean and S. Astilean, *J. Mater. Chem.*, 2011, **21**, 3625.
23 M. Potara, S. Boca, E. Licarete, A. Damert, M. Alupei, M. T. Chiriac, O. Popescu, U. Schmidt and S. Astilean, *Nanoscale*., 2013, **5**, 6013.
24 Y. Yu, Q. Zhang, Q. Yao, J. Xie and J. Y. Lee, *Acc. Chem. Res.*, 2014, **47**, 3530.
25 L. Carbone and P. D. Cozzoli, *Nano Today*, 2010, **5**, 449.
26 C. Wang, W. Tian, Y. Ding, Y.-q Ma, Z. L. Wan, N. M. Markovic, V. R. Stamenkovic,H. Daimen and S. Sun, *J. Am. Chem. Soc.*, 2010, **132**, 6524.
27 J. Gu, Y.-W. Zhang and F. Tao, *Chem. Soc. Rev.*, 2012, **41**, 8050.
28 S. Mourdikoudis, M. Chirea, D. Zanaga, T. Altantzis, M. Mitrakas, S. Bals, L. M. Liz-Marzán, J. Pérez-Juste and I. Pastoriza-Santos, *Nanoscale*, 2015, **7**, 8739..
29 K. Cai, J. Liu, H. Zhang, Z. Huang, Z. Lu, M. F. Foda, T. Li and H. Han, *Chem. Eur. J.*, 2015, **21**, 7556.
30 X. Xia, S.-I. Choi, J. A. Herron, N. Lu, J. Scaranto, H.-C. Peng, J. Wang, M. Mavrikakis, M. J. Kim and Y. Xia, *J. Am. Chem. Soc.,* 2013, **135**, 15706.
31 E. Antolini, *Energy Environ. Sci.*, 2009, **2**, 915.
32 H. Jiang, Z. Chen, H. Cao and Y. Huang, *Analyst*, 2012, **137**, 5560.
33 H. Yi, L.-Q. Wu, W. E. Bentley, R. Ghodssi, G. W. Rubloff, J. N. Culver and G. F. Payne, *Biomacromolecules*, 2005, **6**, 2881.
34 L.-B. Zhao, J.-L. Chen, M. Zhang, D.-Y. Wu and Z.-Q. Tian, *J. Phys. Chem. C*, 2015, **119**, 4949.